Al-Azhar University Civil Engineering Research Magazine (CERM)
Vol. (43) No. (1) January 2021

Assessment of the impact of construction on soil erosion using the revised universal soil loss equation (Case Study-EL-Galalah City)

Abdel Hamid El Tahan[a], Ashraf Elmostafa[b], Ahmed Osama[c], Shokry Abdelaziz[d,e], Lamees Mohamed[f*]

[a] Construction and Building Engineering Department, College of Engineering and Technology-Cairo branch, Arab Academy for Science Technology and Maritime Transport (AASTMT) Cairo, Egypt
[b] Faculty of Engineering, Ain Shams University, Cairo, Egypt
[c] Creative Science and Engineering Department, Waseda University, Tokyo, Japan
[d] Department of Civil Engineering, Faculty of Engineering, King Abdulaziz University, Saudi Arabia
[e] Department of Civil Engineering. Faculty of Engineering, El Mataria, Helwan Univ., Egypt

الملخص العربى:

إن بناء المدن جديدة نشاط بشري مهم يؤثر على البيئة المادية والنظم الإيكولوجية المحيطة به، ويتطلب ذلك إجراء تقييم مناسب للأثر البيئي لمدن الجديدة. في هذه الدراسة، نقوم بتقييم أثر بناء مدينة الجلاله، على هضبة الجلاله، على تآكل التربة باستخدام المعادلة الشاملة المنقحة لفقدان التربة (RUSLE) . ويستخدم التقييم خمسة سيناريوهات مختلفة لسقوط الأمطار سنوياً. وقد جُمعت بيانات المعادلة المختلفة لـ RUSLE على النحو التالي: خرائط التضاريس الأرضية من القمر الصناعى ASTER GDEM ، وخريطة التربة الرقمية للعالم التي قدمتها منظمة الأغذية والزراعة العالميه، ومجموعة بيانات الغطاء الأرضي The Globcover 2009_V2.3 و تبين النتائج أن إجمالي تآكل التربة الحجمي زاد مع زيادة مساحة مستجمعات المياه. وعلاوة على ذلك، أدى بناء المدينة الجديدة إلى انخفاض بنسبة تزيد عن 95٪ في إجمالي تآكل التربة الحجمي في المنطقة. ويهدد انخفاض حجم التربة المنقولة الشواطئ الواقعه على مصب مستجمعات المياه ويشير إلى تراجع الشاطئ بسبب نقص الرواسب التي يتم توفيرها. وهذا بدوره يمكن أن يعرض النظام الإيكولوجي الطبيعي للخطر في أسفل مجرى المستجمعات المائيه في المدينة المنشأة حديثا. ويوفر النهج المقدم للتخفيف من حدة هذه المشكلة طريقة فعالة من حيث التكلفة لتقييم نحات التربة استجابة للتوسع الحضري في المناطق القاحلة وشبه القاحلة، ولا سيما في الشرق الأوسط، حيث توجد خطط لتنمية المناطق الساحلية.

Abstract :

The construction of new urban settlements is a major anthropogenic activity that affects the physical environment and surrounding ecosystems and necessitates an appropriate evaluation of the environmental impact of new settlements. In the present study, we evaluate the impact of the construction of Galalah city, on El-Galalah Plateau, on soil erosion using the Revised Universal Soil Loss Equation (RUSLE). The evaluation uses five different scenarios of annual rainfall. Data for the different RUSLE equation parameters were collected as follows: land topography maps from the ASTER GDEM Satellite, The Digital Soil Map of the World provided by FAOSTAT, and The Globcover 2009_V2.3 Land cover Data set. The results

show that total volumetric soil erosion increased with the increasing watershed area. Moreover, the construction of the new city led to a decrease of more than 95% in the total volumetric soil erosion in the area. The reduction in the transported soil volume threatens downstream beaches and signals the retreat of the shoreline due to lack of supplied sediment. This, in turn, could jeopardize the natural ecosystem downstream of the newly established city. The presented approach to mitigate this problem provides a cost-effective method for evaluating soil erosion in response to urban expansion in arid and semi-arid areas, particularly in the Middle East, where plans to develop coastal areas exist.
Keywords: revised universal soil loss equation (RUSLE) equation, soil erosion, Remote Sensing, environment, GIS, Galalah City, Egypt.

1 Introduction

Soil erosion is a common natural process that affects topography and terrain (Ochoa et al., 2016). Within the field of agriculture, soil erosion denotes the weathering of the topsoil of a field by the natural physical forces of water and wind and/or through forces associated with farming activities, such as cultivation. Erosion, regardless of the causing force, involves three separate stages: soil detachment, movement, and deposition (Toy et al., 2002).

Human activities have risen by 10–40 times the rate at which erosion happens globally (Wilkinson and McElroy, 2007). The most important factors that influence the initiation of the erosion process are industrial agriculture, forestry, highways, anthropogenic activities, and urban sprawl (Blaco and Lal, 2010). Egypt has established new towns and urban settlements in desert areas, and development in the There were several problems confronting the Egyptian desert that were not noticed or measured by developers. The lack of sufficient knowledge of the essence of the desert climate and the position of the social, economic and political environment prevents many new cities in Egypt from developing properly (Ali, 2003). Accelerated urbanization has resulted in soil erosion risks. Urban areas witness rapid economic growth with more construction projects that bring intensive changes to the environment over a short period and add new elements to the erosion system. Therefore, erosion has experienced a more intensive impact from human activities. Therefore, the possible effect of urbanization on soil erosion must be considered when designing or planning to exploit natural resources or to develop urban areas (Hu et al., 2001).

Soil erosion is classified as a global challenge to the natural ecosystem's survival and can be a sluggish process that remains somewhat undetected or happens at a rapid rate, causing significant topsoil depletion (Wood et al., 1994). Topsoil, which is abundant in organic matter (fertility and soil life), is relocated in two instances: "on-site" somewhere where it builds with time, or off-site" is brought where it fills irrigation channels. Soil degradation thus decreases the productivity of croplands and leads to the contamination of nearby rivers, wetlands and lakes (Balasubramanian, 2017). Several erosion models to measure and forecast the erosion and deposition of eroded soil have recently been created. The calibration of these models (classified as scientific, physical, and conceptual) is difficult especially with the limited availability of field data, since the erosion mechanism relies on complex interactions between several parameters. The simplest mathematical models can be extended to circumstances with minimal evidence (Eisazadeh et al., 2012) which include the Bureau of Land Management (BLM) model, the Ephemeral Gully Erosion Model (EGEM), the Universal Soil Loss Equation (USLE), the Revised Universal Soil Loss Equation (RUSLE) and the Modified Universal Soil Loss Equation (MUSLE). Due to their comprehensive structure and extensive availability of input data, the USLE and RUSLE models are the most commonly used (Steinmetz et al., 2018; Igwe et al., 2017) When applying RUSLE for measuring soil erosion, remote sensing is unavoidable in technical environments and helps us to easily obtain knowledge about the progress of erosion processes and to track particular moments and dynamics over time. In addition, for research sites that are difficult to reach or conditions that require overly costly direct field approaches, remote sensing-based methods offer a cost-effective means of examining soil erosion.

In this research, we plan to analyze the effect of Galalah city's establishment on soil erosion along the Gulf of Suez coast using satellite datasets and the Updated Universal Soil Loss Equation (RUSLE) as a case study that can be applied in the Middle East and worldwide to similar settings.

2 Study Area

The study area is situated on the El-Galalah Plateau in the Gulf of Suez between the cities of Al-Ain Al-Sokhna and Zafarana. Newly developed Galalah city lies between 32.475° and 32.325° E longitude and 29.350° and 29.500° N latitude. The city sits at ~650 m above sea level (Fig. 28). The new city is a result of nationwide efforts to develop the vast and lifeless Eastern Desert of Egypt to reduce the congestion of the capital, create work and living opportunities for the youth, and produce investment ventures.

Galalah city is planned on a 170 km^2 plot and adopts a carefully balanced approach towards urban development and preservation of the surrounding original environment. The first phase covers an area of 20.5 km^2, consisting of numerous different activities, such as residential, commercial, touristic village, cultural, medical, educational, and religious buildings.

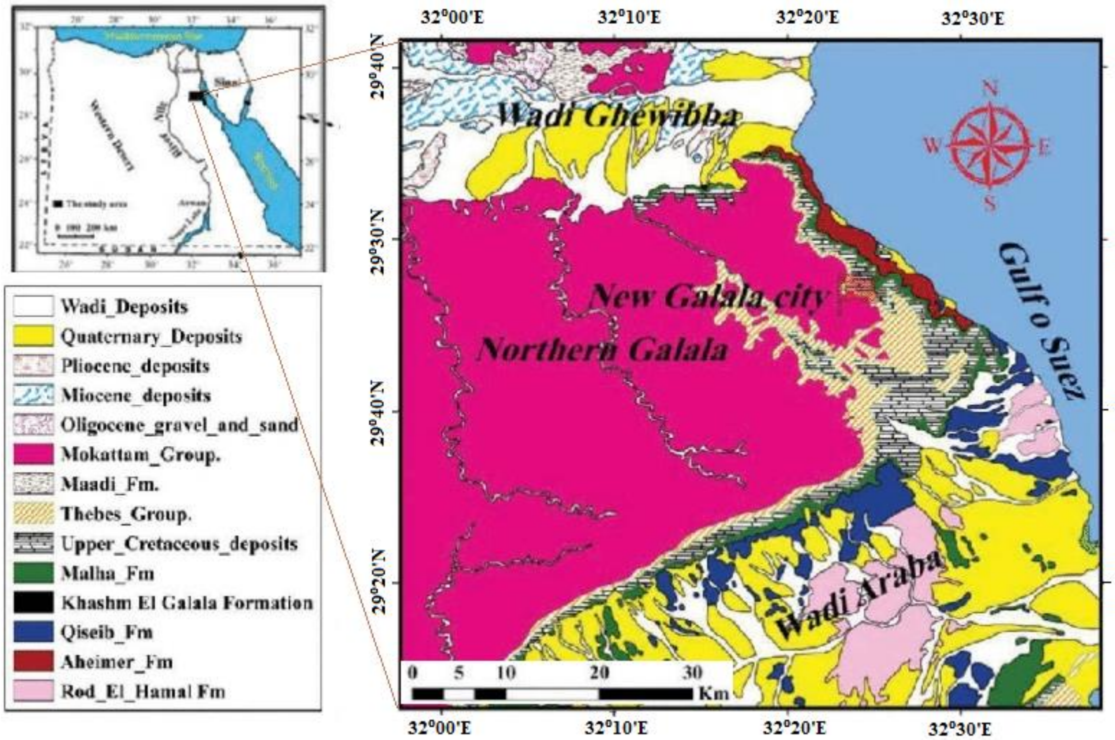

Fig. 28: Location and geological map of the Study Area (modified after Abdelazeem et al. 2019)

The geology of the Northern Galalah plateau has been studied by many researchers such as Sadek (1926), Awad and Abdallah (1966), and Abdallah (1993). Several lithological units cover the studied area ranging from Upper Paleozoic (Permo Carboniferous) and Permo-Triassic to Lower Mesozoic clastics and carbonates (Triassic to Early Cretaceous). This is overlain by marine suites of Cenomanian to Middle Eocene age (Darwish et al. 1984).

As shown in figure 1, the Upper Paleozoic sedimentary units in Wadi Araba, Abu Darag, and Aheimer areas can be grouped to be Rod El Hamal Formation. They classified the rocks exposed at Rod El Hamal, Abu Darag, and Aheimer areas into three formations (The Rod El Hamal Formation, Abu Darag Formation, Aheimer Formation) that are chronologically equivalent. The Permian-Triassic is represented by Qiseib Formation. A clastic portion reflects the Jurassic rocks. Three rock groups, which are from base to top) the Malha Formation, the Galalah Formation, and the chalky limestone and dolomite band, separate the Cretaceous rocks. The rocks from the Paleocene are represented by the Esna Shale. The succession of the Eocene is divided into eight formations; the formations of Farafra, Thebes, Muweilih, Mokattam, Observatory, Qurn, Wadi Garawi and Wadi Hof. Two rock units separate the Oligocene rocks; at the base, the Oligocene sands and gravels (Gebel Ahmar Formation) and at the top, the basaltic layer. At the base and the non-marine Miocene unit at the top, the Miocene rocks are separated into the marine Miocene unit. The unlithified sands and gravels represent the Pliocene. The alluvial deposits of the Pleistocene are represented by (Awad et al. 2017).

Three main systems of faults determine El-Galalah El- Bahariya area include NW- SE direction, E-W system of fractures, and NE-SW direction. The top of the plateau is covered by Sheet basalts. As a result, at contact, the sediments are slightly metamorphosed and marbled calcite and calcite dykes are therefore found at Wadi Haroz, Wadi Ghoul, and Gebel Menedra.From the geomorphological point of view, the area is characterized by the highland, coastal plain, deltas alluvial fan, beaches, sabkhas, and braided channels. The high plateau in Gebel El-Galalah El Bahariya is bounded by scarps and is surrounded on the north by the wide depression of wadi Ghweiba. The coastal plain deposits consist of thick loose deposits and extend parallel to the shoreline of the Gulf of Suez. The area is characterized by boulders, gravel, and sand beach. Several geomorphic features characterize the coastal plain such as deltas, sabkhas, and beaches. The Deltas formed at the ends of the wadis towards the Gulf of Suez are characterized by gradually sloping irregular surface dissected by braided shallow channels and covered by alluvial deposits. The sabkhas lay in elevation mostly less than the sea level and consist of silt, sand, and clay mixed with evaporates formed due to the high evaporation process. The beaches consist of sand and gravel, they have an irregular shape (Mohamed,2001; Awad et al. 2017).

3. Climate Setting

The study area lies in the Eastern Egypt climatic region, which is characterized by a sub-humid climate with two distinct seasons. The first extends from October to April, is humid and cool, contains approximately 85% of annual precipitation, and has an average temperature of approximately 18 °C; the latter extends from May to September and is dry and warm (**خطأ! لم يتم العثور على مصدر المرجع.**) with an average temperature of 25 °C and the average precipitation of 2.5 mm. The prevailing winds blow from the northwest, as illustrated in Fig. **30**.

خطأ! لم يتم العثور على مصدر المرجع. presents the average daily rainfall values over Egypt from 1998–2008 (10 years). The majority of values range between 0.0–50.0 mm over much of the land and peaked at more than 100 mm on the north-west coast and the Red Sea Mountains. The average values over the Red Sea region (where the study area is located) exceed 20 mm per day.

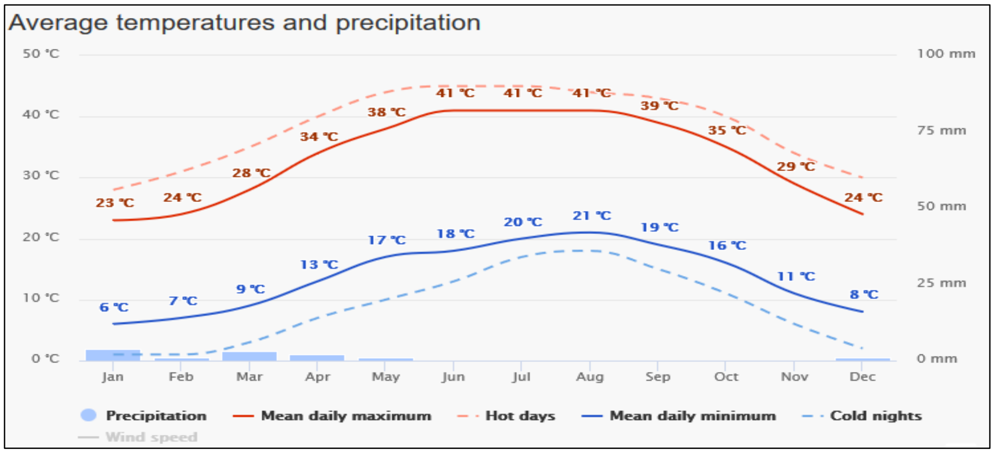

Fig. 29: Temporal Distribution of Average Temperature and Precipitation within the Study Area

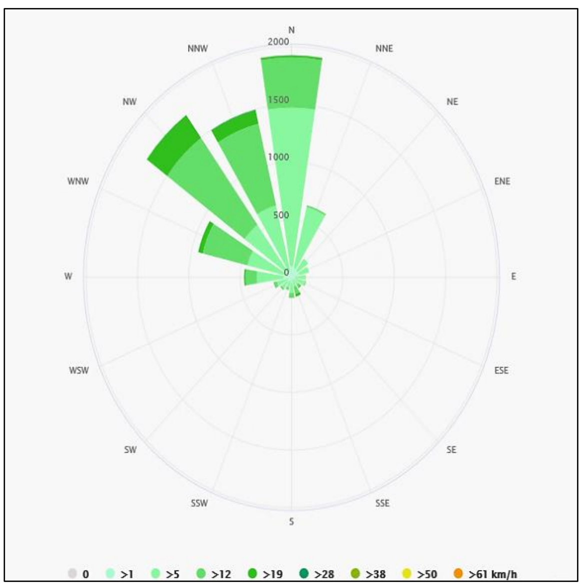

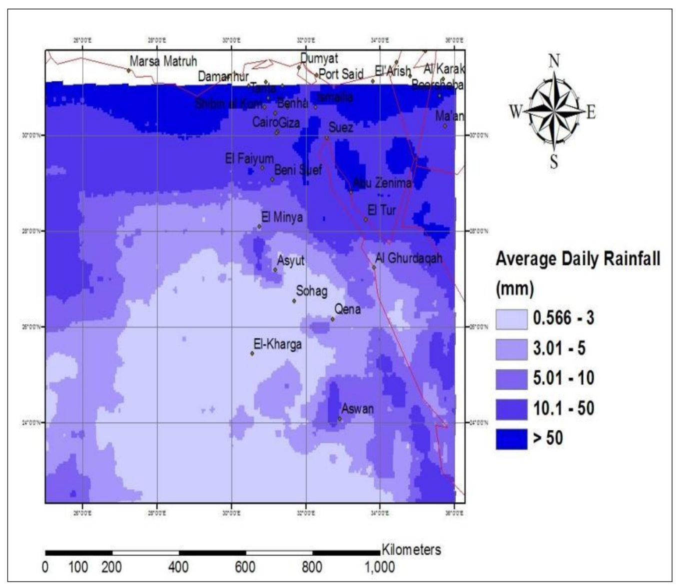

Fig. 30: Wind Rose Showing the Prevailing Wind Direction in the Study Area

Fig. 4: Average rainfall values in Egypt (1998–2008)

4. Data & Methodology

The implemented workflow in this study starts with data collection and assimilation, pre-processing of the data, and extraction of critical information from the input data, namely:

1. Land topography maps from the ASTER GDEM Satellite (NASA, 2009);
2. The Digital Soil Map of the World provided by FAOSTAT (DSMW, 2012);

3. The Globcover2009_V2.3 Land cover Data set (Bontemps et al., 2013);
4. Tropical Rainfall Measuring Mission (TRMM-3B42) (Huffman and Bolvin., 2012)

Three primary data (i.e. ASTER GDEM, DSMW, and Globcover Dataset) were used throughout this study. To explain the topography of the study area, the Advanced Spaceborne Thermal Emission and Reflection Radiometer (ASTER) Global Digital Elevation Model Version 2 (GDEM V2) was employed. Under the supervision of the Ministry of Economy, Commerce and Industry (METI) of Japan and the United States National Government, ASTER GDEM is distributed free of charge. Administration of Aeronautics and Space (NASA). The tiles were downloaded in GeoTIFF format and with 30-meter postings and 1 x 1-degree tiles, adopted the same grids and tile structure as version 1 of the results. The World Database Harmonized Global Soil Map (DSMW) is a 30-arc-second raster database of over 15,000 different soil mapping units integrating current regional and national soil information updates worldwide (SOTER, ESD, Soil Map of China, WISE) with information found within the FAO-UNESCO Soil Map of the World (FAO, 1971-1981) scale of 1:5,000,000.There are 21600 rows and 43200 columns in the resulting raster database that are connected to Harmonized soil property records. The Globcover Dataset is a ground cover classification map provided by the European Space Agency and produced using MERIS satellite imagery in conjunction with the EEA, FAO, GOFC-GOLD, IGBP, JRC and UNEP (Hegazy et al., 2020). The product is based on data from January 2005 to June 2006 from ENVISAT MERIS. There are some 80 classifications in the legend, divided into eight main groups. The file is given in GeoTIFF format and clipped to a legend (Globcover2009 legend.xls) in the EDE Next research area. The colors allocated are rather random, and the layer is intended to provide a basis for each user to assign colors as considered necessary. Data Pre-processing

5.1 Watershed Delineation

The watersheds intersecting the boundary of the study area were delineated using the aforementioned topographic maps. The watershed delineation process addresses the influence of terrain on surface hydrology and the movement of water over the land surface (Fathy et al., 2019), computes the local directions of flow, and defines the stream network, the boundaries between watersheds, and the areas drained by particular stream systems. The ArcGIS hydrology toolkit was used to conduct this process, adopting a threshold of 0.5 km^2 to define the stream network (Fig. 5). A conceptual review of the available satellite images, topographic maps, and digital elevation models revealed that the general slope of the terrain descends eastward as the Red Sea mountain range is situated in the westernmost part of the study area.

The ArcGIS Hydro tools were used to delineate and characterize watersheds in raster and vector formats, to define and analyze hydro geometric networks, to manage time-series data, and to configure and export data to numerical models. The DEM files, satellite images, and geological maps were implemented in the GIS environment to identify the geomorphological parameters (area, longest flow path, slope, etc.) for the watersheds in the study area. The geomorphological characteristics are summarized and presented in **خطأ! لم يتم العثور على مصدر المرجع.**

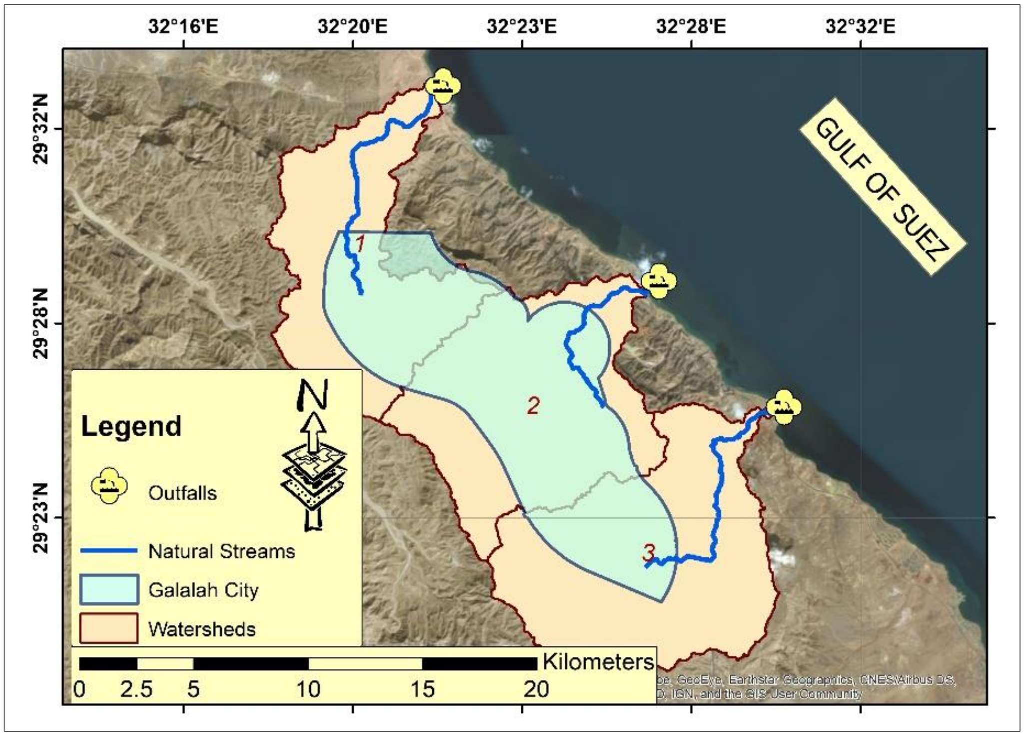

Fig. 5: Delineated Catchments Using ASTER GDEM Draped Over a Satellite Imagery

Table 13: Watershed Morphological Characteristics

Watershed ID	Morphological Parameters			
	Area (km2)	Perimeter (m)	Stream Length (m)	Stream Avg. Slope (m/m)
1	55.8	62.6	12078	12.797
2	66.4	57.7	8674	7.747
3	73.6	59.6	12202	7.153

5.2 The RUSLE

A closer inspection of the Revised Universal Soil Loss Equation (RUSLE) reveals the input data necessary for this investigation. Soil erosion was assessed using the RUSLE in a raster GIS environment to calculate specific factors and annual soil loss in the investigated area. The RUSLE was developed to incorporate new research ideas since the earlier USLE of 1978 (Wischmeier and Smith, 1978; Renard et al., 1997). The RUSLE is as follows:

$$A = R \times K \times LS \times C \times P \qquad (1)$$

Where:

$A =$ the predicted annual soil loss (ton/hectare), $R =$ the rainfall erosivity factor for the target area, $K =$ the soil erodibility factor, $L =$ a dimensionless slope-length factor, $S =$ a dimensionless slope-steepness factor, $C =$ a dimensionless cover and management (or cropping factor), $P =$ a dimensionless conservation practice factor. (Renard et al., 1997)

Rainfall Erosivity Index (R): Erosivity is rainfall's ability to erode the earth. The greater a rainstorm's strength and length, the higher the risk for erosion. Soil aggregates may be broken down and aggregate content spread by the effect of raindrops on the soil surface. The "R" index was determined using the equation:$R = \sum_{i=1}^{12} 1.735 \times 10^{\left(1.5\log_{10}(p_i^2/p)-0.08188\right)}$ (2)

where R is in MJ/mm/ha/h/yr, where p_i is the monthly rainfall in mm, p and is the annual rainfall in mm.

In this research, rainfall was estimated using two methodologies; first, a hypothetical Rainfall was assumed based on the observations in **خطأ! لم يتم العثور على مصدر المرجع.** and **خطأ! لم يتم العثور على مصدر المرجع.** Five cases with a total annual rainfall depth vary from 10 to 50 mm were estimated as indicated in table 2.

Table 2: Hypothetical Rainfall Depth Cases.

Cases	(1)	(2)	(3)	(4)	(5)
Annual Precipitation (mm)	10.00	20.00	30.00	40.00	50.00

Several studies suggest that satellite rainfall data could be used to quantify the rainfall amount with reasonable accuracy especially where ground measurements are minimal (Atif et al. 2020; Tekeli and Fouli, 2016; Matingo et al., 2018). Hence the TRMM 3B42V7 rainfall product used in this study comprises 0.25° × 0.25°grid cell data at a continuous 3 h interval and with spatial coverage of −180 ° W to +180 ° E extending from 50 ° S to 50 ° N latitude. Figure 6 shows the obtained monthly historical rainfall data for the period from 2000 to 2018.

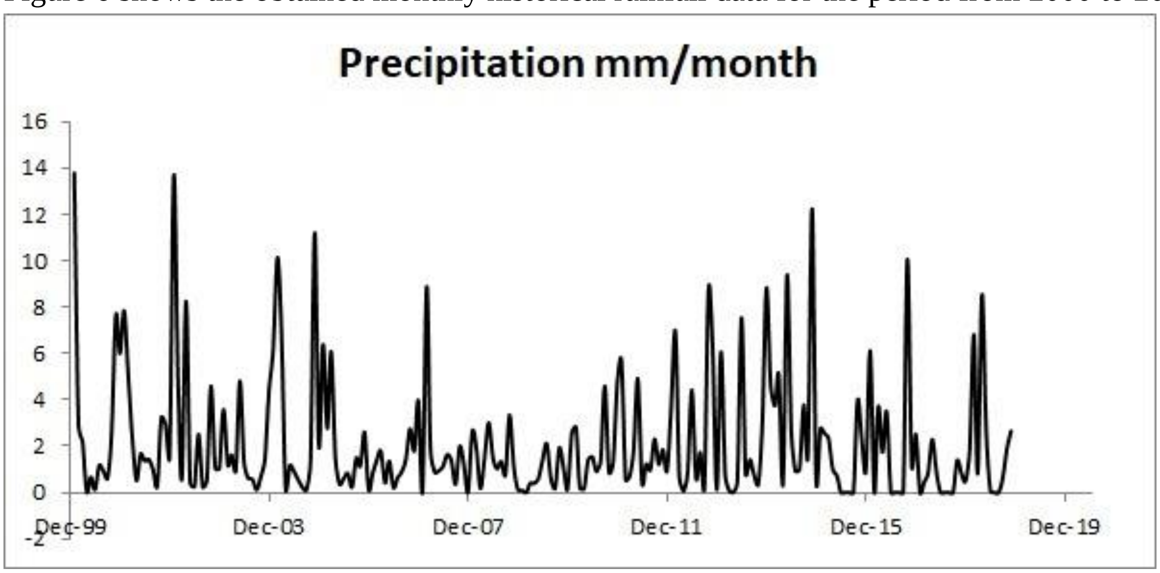

Fig. 6: Historical rainfall TRMM monthly data within the study area

Soil Erodibility Factor (K): The ease with which the soil is detached by splash during precipitation or by surface flow represents this aspect. The erodibility of a given soil is determined by soil texture, organic matter content, structure, and permeability. Because of their resistance to detachment, soils rich in clay have low K values (ranging from 0.05–0.15). Owing to their poor drainage, coarse textured soils, such as sandy soils, have low K values (approximately 0.05–0.2) but are quickly detached. Medium-textured soils have modest K values (about 0.25–0.4), are moderately prone to detachment, and yield moderate drainage, such as silty loam soils. The most erodible are soils of high silt content. They are readily detached, tend to crust and create high runoff rates. This soils appear to have K values greater than 0.4. From the publicly available Harmonized digital soil map of the country, the K index was determined using the following equation published by (Renard et al., 1991).

$$100\ K = 2.1 \times 10^{-4} \cdot M^{1.14} \cdot (12 - a) + 3.25 \cdot (b - 2) + 2.5 \cdot (c - 3) \qquad (3)$$

where K is the soil erodibility factor in t.h/ha/MJ/mm; M is the particle size parameter [(% silt + % very fine sand) (100 - % clay)]; (a) represents organic matter content (%); (b) is the soil structure code; and (c) is the soil permeability class (Fig. 7).

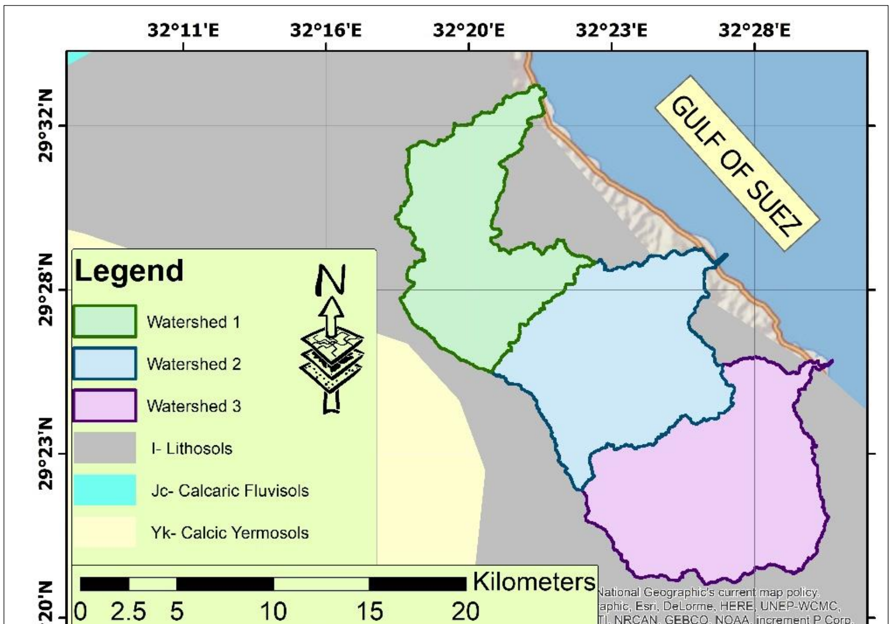

FAOSOIL	sand % topsoil	silt % topsoil	clay % topsoil	OC % topsoil	K USLE	Modified K
Jc25-1ab	39.6	39.9	20.6	0.65	0.619688	0.081613
I-Re-bc	58.9	16.2	24.9	0.97	0.487778	0.064240
Yk20-1ab	63.5	17.9	18.7	0.26	0.616617	0.081208

Fig. 7: Spatial Distribution of Soil Type According to FAOSTAT Dataset.

Topographic factor (LS): Topography impacts the drainage features and sediment distribution mechanisms on a watershed scale (Risse et al., 1993). The slope length factor (L) calculates the erosion influence of slope length, and the slope steepness factor (S) calculates the erosion effect of slope steepness. *Slope length factor (L)*: Using the relationship below, established by

McCool et al, the dimensionless L-factor was determined (1987).$L = (\gamma/22.13)^m$
(4)

where L is the slope length factor, γ is the field slope length (m), m is a dimensionless exponent that depends on slope steepness (0.5 for slopes exceeding 5%, 0.4 for 4% slopes, and 0.3 for slopes less than 3%).

Slope Steepness Factor (S The Dimensionless S-factor for a slope longer than 4 m was determined using the relationship provided by Pandey et al. (2006).

$$S = 10.8 \sin\theta + 0.03 \quad \text{for slopes} < 9\% \quad (5)$$

$$S = 16.8 \sin\theta - 0.5 \quad \text{for slopes} \geq 9\% \quad (6)$$

Where S = the slope steepness factor, and θ = the slope angle in degrees.

The crop management factor (C): The estimated ratio of soil loss from cropped field to soil loss from clean-tilled fallow on the same soil and slope under the same rainfall conditions is the expected ratio. The C-factor illustrates how the maintenance strategy will affect the estimated annual depletion of soil and how the capacity for soil loss will be allocated over time during construction, crop rotations or other management schemes (Figure 8). Based on Rao's work, different values corresponding to different forms of land cover are shown in Table 3 (1981).

The conservation practice factor (P): represents the ratio of soil loss by a support practice to that of straight-row farming up and down the slope and is used to account for the positive impacts of those support practices. The P factor accounts for control practices that reduce the erosion potential of the runoff by their influence on drainage patterns, runoff concentration, runoff velocity, and hydraulic forces exerted by a runoff on the soil. The value of the P factor ranges from zero to one, the value approaching zero indicates good conservation practice and the value approaching one indicates poor conservation practice Ganasri P. H. & Ramesh H. (2016).

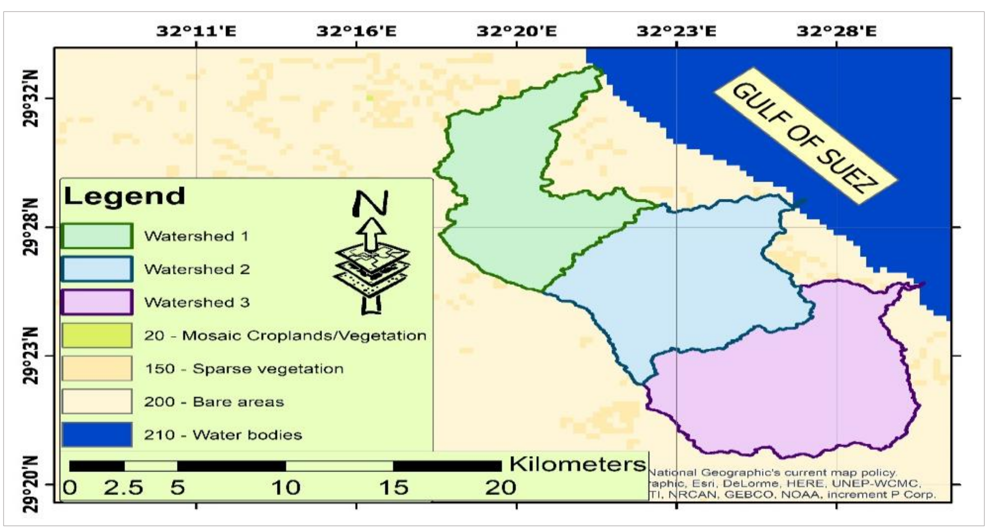

Fig. 8: Spatial Distribution of Land Cover According to Globcover 2009 Dataset

Table 3: Crop Management Factor for Different Land Use/Land Cover Class.

Land Use/Land Cover	Waterbody	Dense forest	Agricultural land	Barren land	Snow	Open forest
C Factor	0.28	0.004	0.28	0.13	0.0	0.008

5. Data Analysis

To evaluate the effect of urban encroachment on the average annual soil erosion two scenarios were considered. the first scenario illustrates the current status of the study area and the second scenario illustrates the statues of the study area after the construction of the Galalah city. It is noteworthy to mention that the aggregated effect of the entire city on the average annual soil erosion was computed and the effect of gradual construction stages was neglected. Furthermore, hypothetical rainfall data was used to ascertain the role of rainfall intensity given the same conditions of land use. Due to the dominance of barren land cover as demonstrated in Figure (8), a constant value of 0.13 was adopted for the Crop Management Factor C; similarly, a constant value for the Erodibility Factor K of 0.06424 was calculated using the FAOSTAT data set (DSMW, 2012) and presented in Figure (7). Besides, a constant value of (1) was adopted for the Conservation Practice Factor as currently no cultivation or any sort of agricultural activity is taking place in the project site Figure (8). As for the future scenario, the value of the Crop Management Factor C varies from 0.45 for bare, idle land to 0.003 for land with ground cover greater than 95 percent. Thus, the authors assumed the Crop Management Factor C to be 0.01. Also, the value for the soil Erodibility Factor K was assumed to be 0.01 which is closer match to the k for limestone (Rozos D. E. 2013) as the construction of the new galalah city has a soil cover which will minimize the soil erosion to a minimum at the study area. Additionally, the conservation practice in the future after urbanization is approximated using the map presented in Figure (10). The Topographic Factor (LS) was computed using a special algorithm that detects the slope and length of the slope using the DEM of the study area then a Spatial Distribution of the LS Factor across the Study Area was produced and presented in Figure (9). The Topographic Factor (LS) remained the same for both the future and current scenario as the land topography will remain the same without changes after the construction process.

After the calculation of all the parameters within the ArcGIS environment, the raster calculator tool was used to produce the average annual soil erosion raster map for the two scenarios; current and in the future Figure (11) and Figure (12).

.

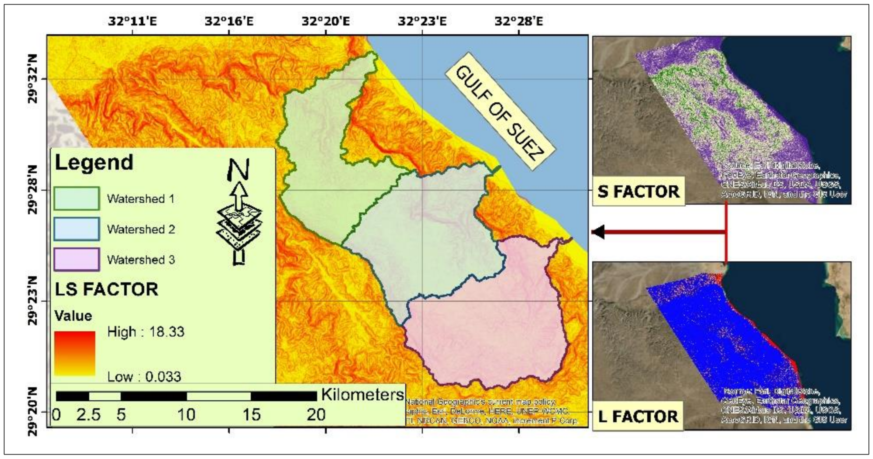

Fig. 9: Spatial Distribution of the LS Factor across the Study Area.

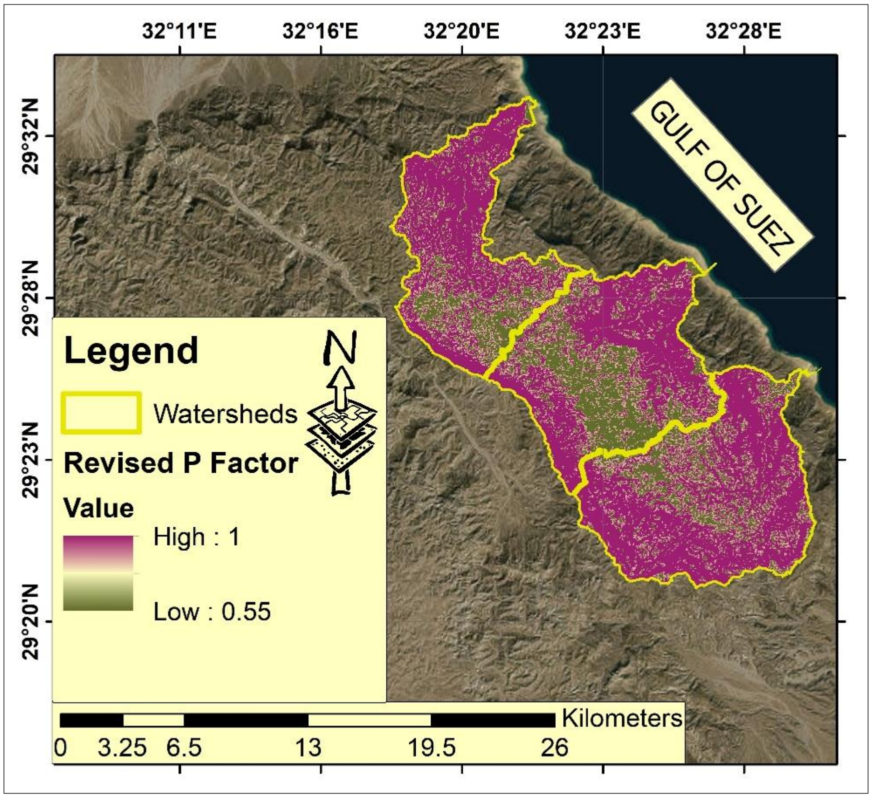

Fig. 310: Spatial Distribution of P Factor across the Study Area - Future Scenario.

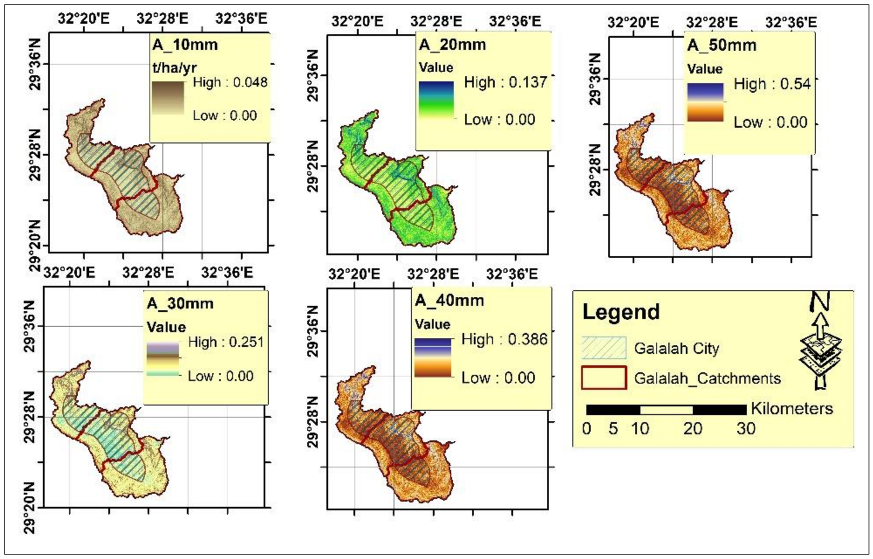

Fig. 321: Spatial Distribution of Soil Erosion across the Study Area – Current Scenario.

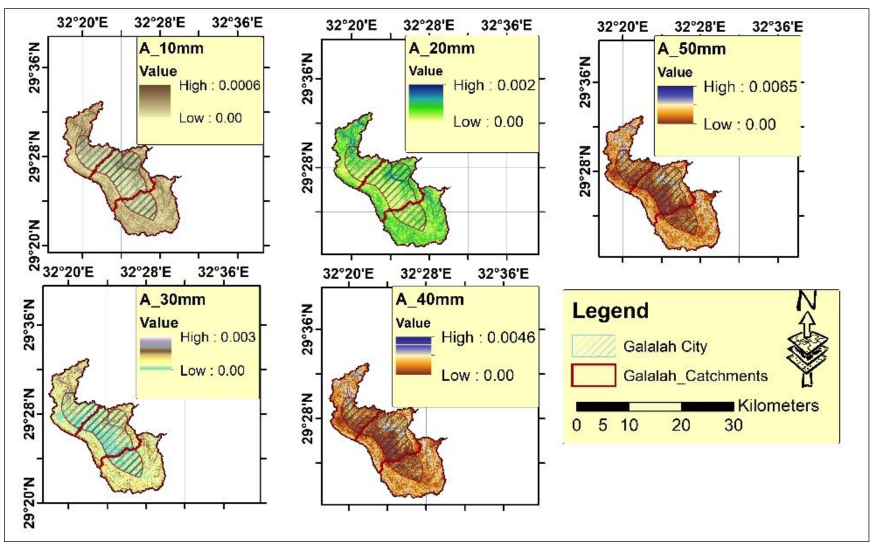

Fig. 33: Spatial Distribution of Soil Erosion across the Study Area – Future Scenario.

According to Naqvi et al. (2013), R is one of the most important factors influencing the soil loss rate. Labib (1981) studied Soil erosion and total denudation due to flash floods in the Egyptian eastern desert where the study area exists, he calculated the R Factor and found it equal to 9.22, which is close to the R factor calculated in different scenarios in this study.

The R factor for 18 years of satellite TRMM data is shown in Figure (13) with an average R factor (7.2). Figure (14) shows the R factor for the five hypothetical rainfall cases as well as TRMM data.

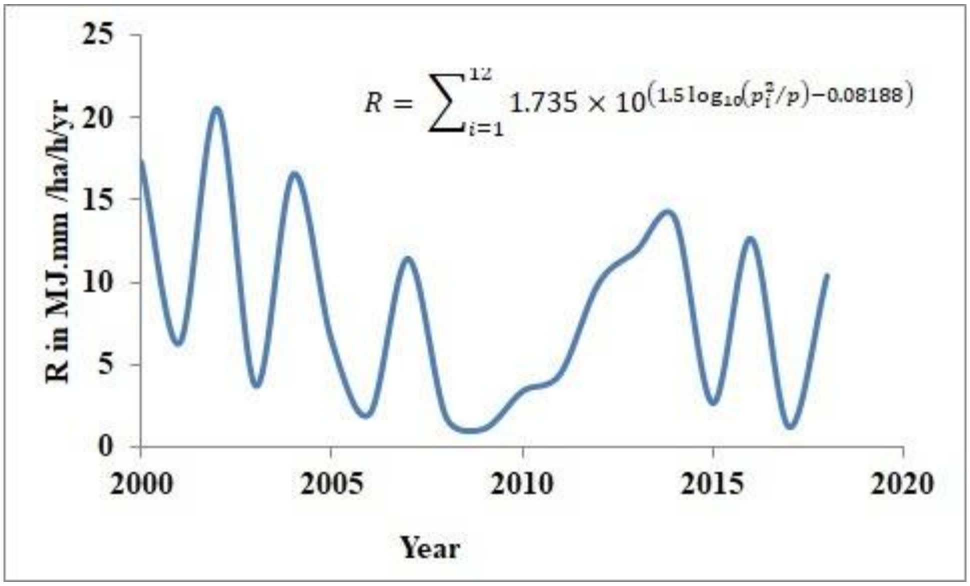

Fig. 13: Annual R Factor based on TRMM data.

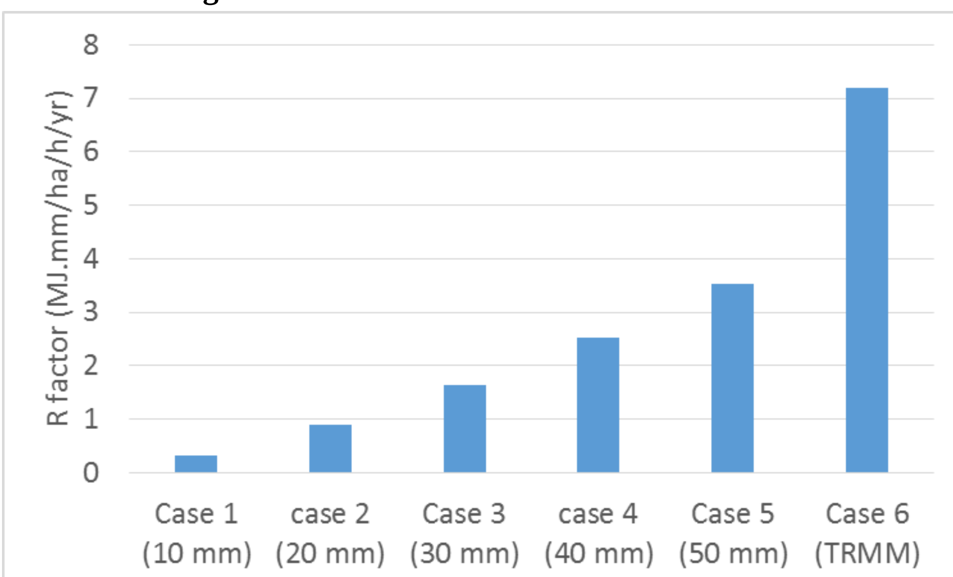

Fig. 14: R Factor for all rainfall cases

6. Results

In this section, the results of the two scenarios and the six rainfall cases will be presented and analyzed. Table 4 and figures 1 and 15 show the results of the current and future scenarios. For the current scenario, the total annual soil erosion is increased dramatically by increasing the rainfall and the watershed area (i.e. the total annual soil erosion is increased from 788.42 ton/ha in watershed 1 and case 1 to 11467.93 in watershed 3 and case 5).

Table 4: Total annual soil erosion in ton/ha for the current and future scenarios.

	Watershed 1		Watershed 2		Watershed 3	
	Current	Future	Current	Future	Current	Future
Case 1	788.42	8.91	820.74	9.15	1025.58	11.59
Case 2	2230.32	25.21	2321.74	25.89	2901.20	32.78
Case 3	4097.28	46.31	4265.23	47.56	5329.75	60.23
Case 4	6308.10	71.29	6566.67	73.23	8205.59	92.72
Case 5	8816.05	99.46	9177.42	102.34	11467.93	129.59
Case 6	17992.47	203.33	18730.04	208.81	23404.68	264.49

Future scenarios with the same annual precipitation are entirely different from the current scenarios, and soil erosion decreased considerably in each watershed. The amount of soil erosion decreased to 8.91, 9.15, and 11.59 ton/ha (annual precipitation of 10.00 mm) in watersheds 1, 2, and 3, respectively. The results of the presented model are matched with the results of wang et. al. (2018) who studied the impact of Urbanization on Soil Erosion in Inner Mongolia, China. Wang et al. (2018) argued that urbanization might reduce soil erosion and thereby ensuring key environmental functions. Unfortunately, there is no historical data for the study area that can be used for model validation; future studies should focus on direct field measurements of soil loss, validating the results estimated according to the RUSLE. (Steinmetz et al., 2018)

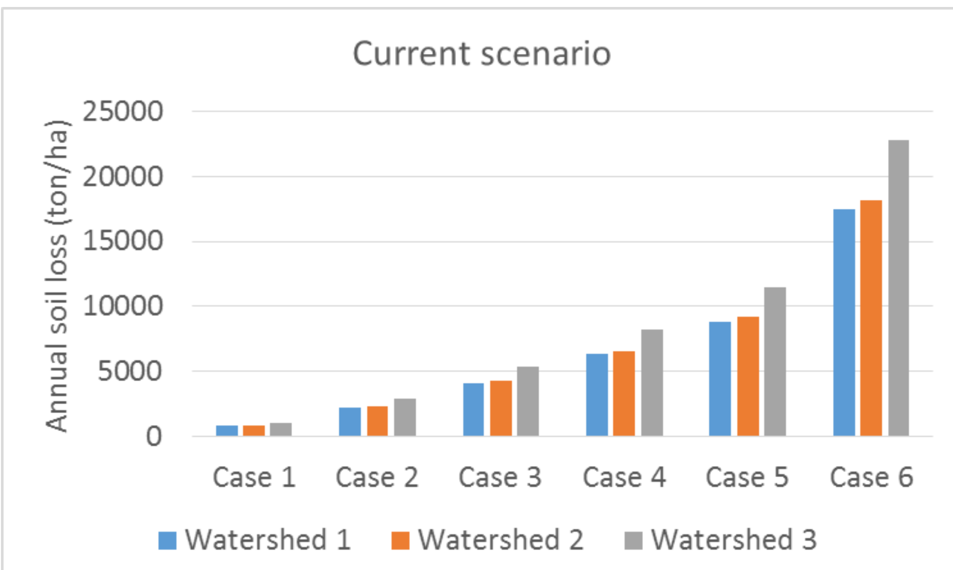

-Fig. 75: Total annual soil erosion in ton/ha for the current

Fig86: Total annual soil erosion in ton/ha for the future scenario.

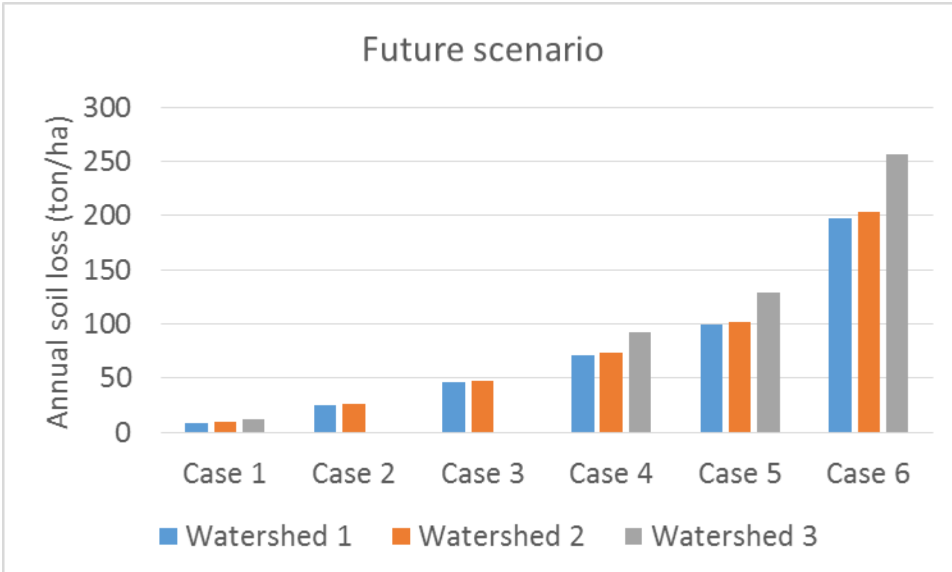

The R factors for 18 years' satellite TRMM data are shown in figure 14. The figure shows that the R factor values vary according to the estimated monthly rainfall between 1 to 20 MJ/mm/ha/h/yr with an average R factor (7.2). Figure 15 shows the R factor for the five hypothetical rainfall cases as well as TRMM data.

7. Discussion

Almost one-quarter of all marine life lives in coral reefs, which are among the most vulnerable and fragile ecosystems. In most countries, coral reefs have been damaged and destroyed by human activities, and if the rate of destruction continues, an additional 60% could be lost in the next 20–40 years (Odyssey Expeditions, 2020). The decrease in sediment supply to the reefs in the study area affects the structure of the reefs; thus, further studies should be conducted to evaluate the positive and negative effects on the reefal environment.

Due to the expected decrease in sediment supply to the shoreline corresponding to Galalah city, the shoreline and marine ecosystem is endangered; hence, a suitable protection method should be used to overcome this risk. Recent methods for coastal erosion mitigation use soft, innovative, and proactive methods that are cheap, construction friendly, and ecofriendly because hard methods have disadvantages for coastal land and beaches (Hegde, 2010). Recommended techniques of road protection, such as Irish crossings, facilitate the transportation of sediments to the sea.

FAO (2017) identified soil erosion by water and wind as the most significant threat to global soils and the ecosystem services they provide and protect. Many studies question the potential of using soil erosion models and claim that more field-based assessment and monitoring of erosion are needed. (Evans, 2013); however, such large-scale erosion assessments require modeling because models can be unscaled to represent large regions. Soil erosion, one of the most severe threats to soils, will not be generally taken into consideration by major environmental and agricultural policy programs (Christine, 2019). Erosion models are tools for understanding, simulating, and predicting (Nearing, 2004) and may serve as an integrating tool for compiling data, knowledge, and observations of different fields (Nearing, 2004). The limitations of the presented model include: (1) the uncertainty of the model results, which arises from the relatively simple empirical approach—suitable for average long-term erosion risk but not for soil erosion under individual rainfall events—, and (2) the failure model to consider antecedent soil moisture and soil stratification. Although the model was first developed for US type soils, numerous studies around the world have demonstrated the ability of the model to capture soil erosion with uncertainty no greater than that found in the US (Yue, 2016).

3. Conclusion

The RUSLE was applied to Galalah city to ascertain the degree to which urbanization contributes to decreasing the total annual erosion volume. Total volumetric soil erosion increased as the watershed area increased. Furthermore, urbanization has decreased the volume of total soil erosion by nearly 95%. The reduction in the transported soil volumes threatens downstream beaches and signals the retreat of the shoreline due to lack of supplied sediment. This, in turn, could jeopardize the natural ecosystem in the vicinity of urban expansion.

Acknowledgments

The authors would like to thank the editor and two anonymous reviewers for their fruitful discussions and significant edits to the manuscript during the review process.

References

Abdallah, A. M., (1993): Structural geology of the area between El-Galalah El-Bahariya and Gebel Okheider, Ph.D. Thesis, Fac., Sci., Ain Shams Univ., Cairo, Egypt, 199 p.

Abdelazeem M., Fathy M. S., Khalifa M. M., (2019). Integrating magnetic and stratigraphic data to delineate the subsurface features in and around new Galala City, Northern Galala Plateau, Egypt. NRIAG Journal of Astronomy and Geophysics, VOL. 8, NO. 1, P. 131–143, https://doi.org/10.1080/20909977.2019.1627634.

Abotalib, A.Z., Sultan, M. and Elkadiri, R., (2016) Groundwater processes in Saharan Africa: implications for landscape evolution in arid environments. Earth-Science Reviews, 156, pp.108-136.

Atif R.M., Siddiqui M.H., Almazroui M., (2020). Near-real-time spatiotemporal analysis of convection and extreme rainfall leading to a flash flood using MSG-SEVIRI and

TRMM data: A case study of a flash flood in Jeddah, Saudi Arabia on November 25, 2009. Vol.13, Issue3,https://doi.org/10.1111/jfr3.12611

Awad M. H, Saad A. M., Draz O. M. and Sakr M. A., (2017) Geotechnical Assessment Of The Soil Foundation In El Galalah El Bahariya Area –North Eastern Desert – Egypt. Al Azhar Bulletin of Science Vol. 9th., Conf., March 2017, p. 89-106

Awad GH, Abdallah AM. 1966. Upper Cretaceous, Eastern Desert, with emphasis on neighboring areas. J Geol UAR. 10(2):125–144.

Blanco-Canqui H., Lal R. (2010) Soil and Water Conservation. In: Principles of Soil Conservation and Management. Springer, Dordrecht. https://doi.org/10.1007/978-1-4020-8709-7_1

Burgess, D. P. (2013). Soil Erosion Threatens Food Production. Journal of Agriculture, 443-463.

Christine, A. P. (2019). Using the USLE: Chances, challenges, and limitations of soil erosion modeling. International Soil and Water Conservation Research, 203-225.

Darwish, M; Abdalla, A.M. and Hassanin, I, M., (1984): Contribution to the petrography and diagenesis of the Jurassic exposures, Gulf of Suez, Egypt. Ann. Geol. Surv. Egypt. Cairo. XIV: 173-192.

DSMW, F.a.A.O.o.t.U. Nations, Editor. (2012), FAO GEO NETWORK: Rome, Italy: FAO.

Eisazadeh L., Sokouti R., Homaee M., Pazira E. (2012): Comparison of empirical models to estimate soil erosion and sediment yield in micro catchments. Eurasian Journal of Soil Science vol (1) p.28 – 33

Evans, R. (2013). Assessment and monitoring of accelerated water erosion of cultivated land - when will the reality be acknowledged? Soil Use and Management, 105-118.

FAO. (2017). Voluntary Guidelines for sustainable soil management food and agriculture organization of the united nations. Retrieved from http://www.fao.org/3/a-bl813e.pdfhttp://www.fao.org/3/a-bl813e.pdf

Fathy, I., Abd-Elhamid, H., Zelenakova, M., Kaposztasova, D. (2019) Effect of Topographic Data Accuracy on Watershed Management. Int J Environ Res Public Health.;16(21):4245. doi:10.3390/ijerph16214245

Ganasri P. H. & Ramesh H. (2016) Assessment of soil erosion by RUSLE model using remote sensing and GIS - A case study of Nethravathi Basin. Geoscience Frontiers Volume 7, Issue 6, November 2016, Pages 953-961.

Hegazy, D., Abotalib, A.Z., El-Bastaweesy, M., El-Said, M.A., Melegy, A. and Garamoon, H., (2020) Geo-environmental impacts of hydrogeological setting and anthropogenic activities on water quality in the Quaternary aquifer southeast of the Nile Delta, Egypt. Journal of African Earth Sciences, 172, p.103947.

Hegazy, I, Moustafa, W. (2013) Toward revitalization of new towns in Egypt case study: Sixth of October. International Journal of Sustainable Built Environment., 2(1), 10-18

Hegde, A. V. (2010). Coastal erosion and mitigation methods – Global state of art. Indian Journal of Geo-Marine Sciences, 521-530.

Hu, S., Zhi-mao, G. & Jun-ping, Y. The impacts of urbanisation on soil erosion in the Loess Plateau region. (2011) J. Geogr. Sci. 11, 282–290. https://doi.org/10.1007/BF02892311

Huffman GJ, Bolvin DT. (2012). TRMM and other data precipitation data set documentation. ftp://precip.gsfc.nasa.gov/pub/trmmdocs/3B42_3B43_doc.pdf.

Igwe, P.U.; Onuigbo, A.A; Chinedu, O.C; Ezeaku, I.I.; Muoneke, M.M. (2017): Soil Erosion: A Review of Models and Applications. International Journal of Advanced Engineering Research and Science (IJAERS) Vol-4, Issue-12

Labib, T. M. (1981). Soil erosion and total denudation due to flash floods in the Egyptian eastern desert. Journal of Arid Environments, 4: 191-202.

M.K. Doula, A. S. (2016). Chapter 4 - Soil Environment. In V. J. Stavros G. Poulopoulos, Environment and Development (pp. 213-286). Elsevier.

Matingo T., Gumindoga W., Makurira H., (2018). Evaluation of sub-daily satellite rainfall estimates through flash flood modeling in the Lower Middle Zambezi Basin. Proc. IAHS, 378, 59–65, https://doi.org/10.5194/piahs-378-59-2018

McCool, D.K., et al., (1987) Revised slope steepness factor for the Universal Soil Loss Equation. American Society of Agricultural Engineers.

Mohamed, U.A.A., (2001): Geophysical studies on Wadi Hagul- Wadi Bada area, North of AinSokhna, Gulf of Suez. Ph.D. Thesis, Fac. Sci., Mansoura Univ., Egypt

NAQVI, H. R. et al. (2013.) Multi-temporal annual soil loss risk mapping employing the Revised Universal Soil Loss Equation (RUSLE) model in Nun Nadi Watershedm Uttrakhand (India). Arabian Journal of Geosciences, 6(40):4045-4056.

NASA/METI/AIST, ASTER (2009) Global Digital Elevation Model, a.U.S.J.A.S.T. Japan Spacesystems, Editor. NASA EOSDIS Land Processes DAAC.

Nearing, M. (2004). Soil Erosion and Conservation. In M. M. John Wainwright, Soil erosion and conservation. Finding Simplicity in Complexity (pp. 277-290). West Sussex P: John Wiley & Sons, Ltd.

Ochoa, A., et al., (2016) Effects of climate, land cover, and topography on soil erosion risk in a semiarid basin of the Andes. CATENA, 140, 21-42

Odyssey Expeditions. (2020). marine biology. Retrieved from https://www.marinebiology.org/coralreefs.htm

Pandey, A., V.M. Chowdary, and B. Mal,(2006) Identification of critical erosion-prone areas in the small agricultural watershed using USLE, GIS, and Remote Sensing. Water Resources Management,. 21(4): p. 729-746.

Radoux, Julien & Bontemps, Sophie & Defourny, Pierre & Eric, Van & Lamarche, Céline & Frédéric, Achard & Mayaux, Philippe & Martin, Boettcher & Brockmann, Carsten & Kirches, Grit & Martin, Zülkhe & Kalogirou, Vasileios & Seifert, Frank Martin & Arino, O. . (2013). Consistent Global Land Cover Maps for Climate Modelling

Communities: Current Achievements of the ESA' Land Cover Cci. in ESA Living Planet Symposium. Edinburgh, United Kingdom.

Rao, Y.P. (1981) Evaluation of cropping management factor in universal soil loss equation under natural rainfall condition of Kharagpur, India. in Southeast Asian regional symposium: Problems of soil erosion and sedimentation. Asian Institute of Technology, Bangkok.

Rateb, A. and Abotalib, A.Z., (2020) Inferencing the land subsidence in the Nile Delta using Sentinel-1 satellites and GPS between 2015 and 2019. Science of The Total Environment, p.138868.

Renard, K.G., et al., (1991) RUSLE "revised universal soil loss equation". Soil and Water Conservation,. 46: p. 30-33.

Renard, K.G., et al., (1997) Predicting Soil Erosion by Water: A Guide to Conservation Planning with the Revised Universal Soil Loss Equation (RUSLE) p.404, in Agricultural Handbook No. 703., B.P.S. Analysis, Editor., Resources and Arid Environments: USDA, Washington DC. p. 83-91.

Risse, L.M., et al.,(1993) Error assessment in the universal soil loss equation. American Journal for Soil Scientific Society. 57: p. 825-833.

Rozos D. E., Skilodimou H. D., Loupasakis C., Bathrellos G. D., (2013) Application of the revised universal soil loss equation model on landslide prevention. An example from N. Euboea (Evia) Island, Greece. Environmental Earth Sciences Vol.70 P.3255–3266, DOI: 10.1007/s12665-013-2390-3

Sadek H. 1926. The geography and geology of the district between Gebel Ataqa and El Galalah El Bahariya (Gulf of Suez). Egypt: Geol. Surv. Min. Res. Dept.; p. 120.

Steinmetz A., Cassalho F., Caldeira T., Augusto de Oliveira V., Beskow S., Timm L. (2018): Assessment of soil loss vulnerability in data-scarce watersheds in southern Brazil. Ciência e Agrotecnologia, 42(6):575-587

Tekeli A. E., Fouli H.(2016). Evaluation of TRMM satellite-based precipitation indexes for flood forecasting over Riyadh City, Saudi Arabia. Journal of Hydrology, Vol.541, P.471-479, ISSN 0022-1694

Toy, T.J., G.R. Foster, and K.G. Renard, (2002) Soil Erosion: Processes, Prediction, Measurement, and Control. : John Wiley & Sons.

Tsegaye, B. (2019). Effect of Land Use and Land Cover Changes on Soil Erosion in Ethiopia. Agriculture Science and Food Technology, 026-034.

Wang L.Y, Xiao Yi, Rao E.M., Jiang L., Xiao Y., Ouyang Z. Y. (2018): An Assessment of the Impact of Urbanisation on Soil Erosion in Inner Mongolia. Int. J. Environ. Res. Public Health 2018, 15(3), 550; https://doi.org/10.3390/ijerph15030550.

Wilkinson, H.B, McElroy, J, B. The impact of humans on continental erosion and sedimentation. (2007). GSA Bulletin, 119, no. 1/2, 140–156; DOI: 10.1130/B25899.1

Wischmeier, W.H., and D.D. Smith, (1978) Predicting Rainfall Erosion Losses from Cropland East of the Rocky Mountains, in Agricultural Handbook.: USDA, Washington, DC.

Wood, M.K., et al., (1994) Variations in plants, soil, water, and erosion in pinyon pine and juniper dominated range site, in the variability of Rangeland Water Erosion Processes., SSSA. p. 93-106.

Yue, Y. N. (2016). Lateral transport of soil carbon and land-atmosphere CO2 flux induced by water erosion in China. Proceedings of the National Academy of Sciences of the United States of America, (pp. 6617-6622.). The United States of America.